Hearing Research 443 (2024) 108951

Contents lists available at ScienceDirect

Hearing Research

journal homepage: www.elsevier.com/locate/heares

Research Paper

Regional differences in cochlear nonlinearity across the basal organ of Corti of gerbil
Regional differences in cochlear nonlinearity

C. Elliott Strimbu [a], Lauren A. Chiriboga [b], Brian L. Frost [c], Elizabeth S. Olson [a,b,*]

[a] Department of Otolaryngology, Head and Neck Surgery, Columbia University Vagelos College of Physicians and Surgeons, 630 West 168th Street, New York City, NY 10032, USA
[b] Department of Biomedical Engineering, Columbia University, 1210 Amsterdam Avenue, New York City, NY 10027, USA
[c] Department of Electrical Engineering, Columbia University, 500 West 120th Street, New York City, NY 10027, USA

ARTICLE INFO

Keywords:
Outer hair cell
Cochlear amplifier
Deiters cell
Hair cell
Cochlea
Gerbil

ABSTRACT

Auditory sensation is based in nanoscale vibration of the sensory tissue of the cochlea, the organ of Corti complex (OCC). Motion within the OCC is now observable due to optical coherence tomography. In a previous study (Cooper et al., 2018), the region that includes the electro-motile outer hair cells (OHC) and Deiters cells (DC) was observed to move with larger amplitude than the basilar membrane (BM) and surrounding regions and was termed the "hotspot." In addition to this quantitative distinction, the hotspot moved qualitatively differently than the BM, in that its motion scaled nonlinearly with stimulus level at all frequencies, evincing sub-BF activity. Sub-BF activity enhances non-BF motion; thus the frequency tuning of the OHC/DC region was reduced relative to the BM. In this work we further explore the motion of the gerbil basal OCC and find that regions that lack significant sub-BF activity include the BM, the medial and lateral OCC, and the reticular lamina (RL) region. The observation that the RL region does not move actively sub-BF (already observed in Cho and Puria 2022), suggests that hair cell stereocilia are not exposed to sub-BF activity in the cochlear base. The observation that the lateral and RL regions move approximately linearly sub-BF indicates that linear forces dominate non-linear OHC-based forces on these components at sub-BF frequencies. A complex difference analysis was performed to reveal the internal motion of the OHC/DC region and showed that amplitude structure and phase shifts in the directly measured OHC/DC motion emerge due to the internal OHC/DC motion destructively interfering with BM motion.

1. Introduction

Phase-sensitive optical coherence tomography (OCT) has allowed observations of motion within the sensory tissue of the organ of Corti complex (OCC). Before OCT, observations were restricted to the first-encountered surface of the organ, which is the basilar membrane (BM) in the basal, high-frequency, region discussed in this report. Decades of observations revealed and confirmed that in healthy cochleae, frequency tuning at an auditory neuron is much like that of BM motion (Narayan et al., 1998). BM motion is nonlinear (it scales compressively with sound level) likely due to active outer-hair-cell (OHC)-based forces driven by mechano-electric transduction (MET) current. The MET current saturates, leading to nonlinear OHC-based force (Fettiplace and Kim, 2014; Iwasa and Adachi, 1997). Thus, the non-linear motion is "active" motion. At the BM, activity was limited to frequencies near the best frequency (BF) of the measurement location, where *post-mortem* motion was reduced by factors approaching 1000 at low sound pressure levels (SPL) (Rhode, 2007). (BF is the frequency where motion peaks at low SPL; and BF was determined at the lowest SPL where the peak could be identified.) The OHC electro-mechanical transduction that is presumed responsible for the *in vivo* activity is not tuned when measured in isolated OHCs (Frank et al., 1999) and the basis for the frequency tuning of nonlinear, active motion *in vivo* is not known, although creative cochlear models can predict this tuning (for example, Nankali et al. 2020, Yoon et al. 2011).

OCT-based measurements revealed motions in the OHC region of the sensory tissue that were greater than BM motion (at all frequencies at low-moderate SPL, and sub-BF at high SPL), leading to the term

* Corresponding author.
E-mail address: eao2004@columbia.edu (E.S. Olson).

https://doi.org/10.1016/j.heares.2024.108951
Received 14 July 2023; Received in revised form 7 January 2024; Accepted 11 January 2024
Available online 12 January 2024

"hotspot" for the OHC/DC region (Cooper et al., 2018). The aptness of the term is clear in the motion maps from a healthy gerbil cochlea, as seen in Fig. 1C–F. Multitone stimuli were used, and displacement gain maps are shown at 40 dB SPL (C and D) and 67 dB SPL (E and F), at the BF (D and F) and BF/2 (C and E). Corresponding phase maps are in Fig. 1G–J. As will be shown in later figures, motion within the OHC/DC region also differed from the BM by showing active, nonlinear motion at sub-BF frequencies (Cooper et al., 2018). Sub-BF nonlinearity appeared at relatively low SPL when multitone stimuli were used, likely because the simultaneous presence of near-BF tones led to saturation of MET current at low-moderate SPL. The presence of sub-BF activity can also be identified when sub-BF responses are reduced *post-mortem* (Strimbu et al., 2020; He et al., 2018; Cho and Puria, 2022). OHC-generated current is nonlinear (both at BF and sub-BF) at moderate SPL with multitone stimuli and is nonlinear sub-BF at high SPL with single-tone stimuli, reaffirming the expectation that nonlinearity in motion responses is due to MET current saturation (Fallah et al., 2019; Dong and Olson, 2013, 2016).

The presence of sub-BF activity in the OHC region is consistent with the untuned character of electromotility. However, because it elevates non-BF responses, sub-BF activity results in diminished tuning in the OHC region compared to the tuning at the BM. With this paper we note regional differences in sub-BF activity across the basal OCC, to explore the degree to which OHC sub-BF activity impacts the motion lateral to the OHCs, and within the RL region. Understanding what regions are subject to OHC sub-BF activity is key to understanding what the mechanical stimulus to stereocilia is and impacts the basic cochlear mechanical question of how BF tuning works in the cochlear base.

2. Methods

Animal preparation: The experiments were approved by the Institutional Animal Care and Use Committee of Columbia University. Adult gerbils of both sexes were used. They were initially anesthetized with intraperitoneal (IP) injections of 40 mg/kg ketamine and 40 mg/kg sodium pentobarbital. Buprenorphine, 0.1 mg/kg, was administered at the start of the surgery and after 6–8 h. Supplemental doses of pentobarbital were administered to maintain areflexia in response to a toe pinch. Some animals were also given subcutaneous injections of 2 % lidocaine. The animals were tracheotomized to facilitate breathing and their temperatures were maintained with a heating blanket. Supplemental heating was provided by a lamp and disposable hand warmers. The head was attached to a goniometer and the pinna and most of the cartilaginous ear canal (EC) and tissue covering the temporal bones were removed. The bulla was gently opened with forceps. At the end of the experiment the animals were euthanized with pentobarbital. Animal numbering is for internal record keeping.

Stimulation and response recording: Acoustic stimuli were generated by a Tucker Davis Technologies system and were presented closed-field to the EC by a Radio Shack dynamic speaker. A Sokolich ultrasonic microphone (WGS & Associates, Newport Beach, CA) was coupled to the speaker tube for sound measurement just inside the EC. Measurements were recorded at 98 kHz (97,656.25 Hz) or 130 kHz (130,208.33 Hz). The multitone stimuli used here were zwuis tone complexes in which N frequencies are played simultaneously (van der Heijden and Joris, 2003). The frequencies were chosen to have an integer number of cycles in the recording window, approximately equal spacing (up to a few percent), and had no harmonics or intermodulation distortion products up to third order. Each sinusoidal component of the complex was assigned a random phase so the total sound pressure level, in dB SPL, was ~ 10 log N higher than each individual frequency component. The number of frequencies and frequency ranges are indicated in the figure legends. Multitone stimuli were 1 s in length except for the data in Fig. 9, which was 10 s. Single-tone stimuli were presented as discreet sweeps in which each frequency was presented for 63 ms including a 1 ms rise/fall tapered with a cosine-squared envelope. Single-tone stimuli were played with a higher maximal level to cover the same dynamic range as the multitone stimuli. Single-tone sweeps were 2 s total in length.

OCT: Displacement measurements were acquired using a Thorlabs Telesto 320 spectral domain OCT system with a central wavelength of 1300 nm. OCT produces a 1-D "image" within the depth of the preparation, which is termed an axial scan (A-scan); scanning with mirrors

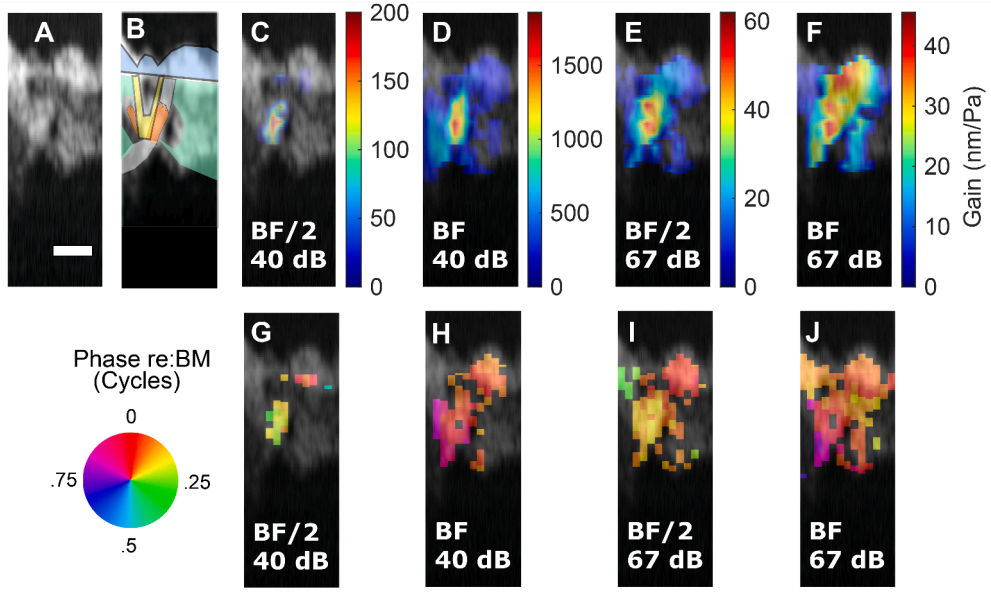

Fig. 1. A. Brightness-scan (B-scan). The white regions are regions that reflect the OCT light, the dark regions are fluid spaces. The scale bar is 50 μm. B. B-scan with transparent cartoon of approximate anatomy with blue the BM, yellow the pillar cells, orange the outer and inner hair cells (OHC/IHC to the right/left of pillar cells). The white transparent regions below and above the OHCs are the tectorial membrane (TM) and Deiters cells, respectively. (See Fig. 2A for detailed labelling of a radial-transverse cross section.) C–D Motion response heatmaps for 40 dB SPL multitone stimuli at BF/2 and BF. Displacements are plotted as gain (nm/Pa). G–H corresponding phase relative to BM motion. E-F Motion response heatmaps for 67 dB SPL multitone stimuli, at BF/2 and BF. I–J corresponding phase, relative to BM motion. The longitudinal, radial and transverse components of the optical axis were 0.85, 0.24, 0.47. Gerbil 995 run 23. Frequency responses from this run are in Fig. 10.

along a second axis produces a 2-D image termed a B-scan. Moving the scanning mirrors in a third, orthogonal direction, the instrument can construct a 3-dimensional volumetric scan. The ThorImage program was used to generate B-scans to orient the preparation and locate the regions of interest within the cochlea, and for volumetric (3-D) imaging. The OCT system is equipped with an LSM03 objective lens, and the properties of the light source and lens determine the system's imaging resolution. The system has an axial resolution of approximately 4 μm and a lateral resolution of approximately 10 μm. The vertical positions of measurement locations in a B-scan are noted in pixels, and the distance between adjacent pixels is 2.7 μm.

Acquisition and initial processing of the OCT vibrometry data were performed using custom software written in C++ using the Thorlabs Spectral Radar software development kit. Later analysis used scripts developed in Matlab.

Experimental design: The initial M-scans along a single A-scan axis were typically made close to the intersection of the arcuate and pectinate zones, passing through the outer hair cell region. B-scan area-spanning recordings of the uniaxial vibrations were constructed by taking sequential M-scans in 10 μm quasi-radial steps, termed "slices". To confirm that the structures were stable over the length of the recordings, the OCT software took B-scans of the same region before and after each set of vibration measurements and we compared the two images to exclude recordings with significant drift.

Each M-scan has a corresponding A-scan image, and time waveforms were extracted from points corresponding to local maxima in the A-scan, following Lin et al. (2017). Once the time-domain displacement waveforms were acquired for the pixels of interest, the amplitudes and phases at the sound stimulus frequencies were extracted by Fourier analysis. For each stimulus frequency, the response was deemed significant if the Fourier coefficient was 3 times larger than the standard deviation of the noise level, measured from 10 neighboring bins in the spectra. Further, for the evaluation of this report, responses were included when they were detectable at BF/2 down to 67 or 70 dB SPL, so that the gain metrics defined below could be evaluated. The signal-to-noise level depends strongly on the local reflectivity of the tissue, and locations deeper and more lateral within the OCC were generally less reflective than the BM and RL region, so are reported relatively sparsely.

Responses are reported as gain relative to ear canal compressional pressure in nm/Pa (amplitude) and cycles (phase). The motion measurement axis is along the optical axis, with the positive direction away from the OCT optics. This report includes OCT-observations made over several years in several studies. None of the specific data here were previously published. A common aspect of experimental design was to simultaneously observe motion at different locations within the sensory tissue of the OCC. The studies sometimes pursued specific hypotheses, for example regarding the effect of ototoxic drugs (Strimbu et al., 2020, 2022), but the results here are of unperturbed cochleae.

3. Analytical methods

Longitudinal, radial, transverse components of the optical axis: Frost et al. (2022) outlined a program in which a volume scan is used to generate the mapping between anatomical coordinates (the longitudinal (L), radial (R) and transverse (T) directions noted in Fig. 2A) and optical coordinates from an OCT volume scan. When volume scans were taken, L, R, T components of the optical axis are reported. The relative values of these components indicate how much each of these directions is represented in the measured motion. For example, in Fig. 4, the relative L, R, T components were 0.85, 0.24, 0.47, signifying that the optical axis was primarily in the longitudinal direction but with substantial radial and transverse contributions. (Two significant figures are excessive for these results but are retained for clarity so the components sum in quadrature to ~ 1.) Motion along any of the anatomical axes would contribute to the displacement measurement, with the actual motion in each anatomical direction weighted by its respective signed component in the measured motion.

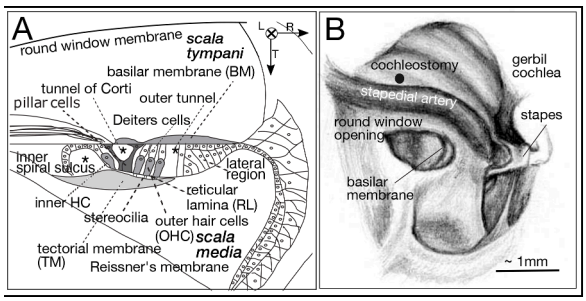

Fig. 2. A. Cartoon of a cross section of the gerbil cochlear base; a transverse-radial B-scan gives this view. Longitudinal, radial and transverse directions are defined (L,R,T). The longitudinal direction points along the spiral of the cochlea, from the base towards the apex. Asterisks note the fluid tunnels that appear as dark areas and help parse the anatomy in a B-scan. B. Left gerbil cochlea. Motion measurements were made through the RW membrane, either with the optical axis transverse, in the very basal region, or pointing down the cochlear spiral to reach a lower BF region, with the optical axis including significant longitudinal, transverse and sometimes radial components. One measurement was made through a cochleostomy with placement as indicated.

3.1. Metrics related to quantifying sub-BF activity

Metrics are defined to support the division into sub-BF-active and sub-BF-not-active (or insignificantly-active) regions. As will be discussed with respect to Fig. 4, the metrics were applied to data taken with multitone stimuli. The following measured quantities are used:

- The response gain at BF, measured at 70 dB SPL, G_{BF70}.
- The response gain at BF/2, measured at 70 dB SPL, $G_{0.5BF70}$ (In gerbil 995 the measurements were done at 67 instead of 70 dB SPL, and 67 dB SPL data are used.)
- The response gain at BF/2, measured at 80 dB SPL, $G_{0.5BF80}$.

Our first metric for assessing sub-BF activity is *GR1*:

$$GR1 = \frac{G_{0.5BF70}}{G_{0.5BF80}}$$

If sub-BF nonlinearity is perfectly absent, $GR1 = 1$. If compressive nonlinearity is present, $GR1 > 1$. In the analysis, *GR1* was never exactly equal to 1 and we choose a value of 1.3 as a cut-off, with *GR*1 values greater than 1.3 showing sufficient nonlinearity to be considered sub-BF active. $GR1 < 1$ corresponds to expansive nonlinearity and when it was indicated it was likely due to signal-to-noise limitations; robust expansive nonlinearity was not apparent. The *GR1* metric was sometimes ambiguous, for example due to local notches occurring at BF/2, leading us to define a second metric, *GR2(dB):*

$$GR2(dB) = 20log_{10}\left(\frac{G_{0.5BF70}}{G_{BF70}}\right)$$

The rationale for *GR2(dB)* and its logarithmic form are as follows: At moderate-high SPL (67 or 70 dB), locations that show sub-BF nonlinearity (amplified gain) have elevated gain at BF/2, and often have reduced gain at BF — when extreme, this was termed "hypercompression" (Cooper et al., 2018). The result is that at these locations $\left(\frac{G_{0.5BF70}}{G_{BF70}}\right) > 1$. In contrast, locations that do not show sub-BF nonlinearity typically have higher gain at BF than BF/2, and $\left(\frac{G_{0.5BF70}}{G_{BF70}}\right) < 1$. We take the logarithm (presented as dB value) because that divides sub-BF apparently active and sub-BF apparently not-active into positive and negative $GR2(dB)$ values respectively. Table 1 lists the *GR1* and *GR2(dB)* values. Of 138 *GR1* values, 102 (74 %) had values < 1.4, indicating lack of significant sub-BF nonlinearity. Of these 102, 97 (95 %) had *GR2* values

Table 1
GR1 and GR2 metrics defined in methods arranged by animal number, run (r) number, slice (sl) number and pixel number.

ID	Pixel	GR1	GR2(dB)	ID	Pixel	GR1	GR2(dB)	ID	Pixel	GR1	GR2(dB)
G986 r4	51	1.0	-4	G995 r23 sl3	157	1.0	-6	G995 r23 sl9	166	0.9	-5
G986 r4	53	1.2	-3	G995 r23 s 3	174	2.1	0	G995 r23 sl9	185	0.7	-5
G986 r4	55	1.3	-3	G995 r23 sl3	178	2.5	1	G995 r23 sl9	196	1.0	-1
G986 r4	60	0.8	-7	G995 r23 sl3	186	1.8	-4	G995 r23 sl10	150	0.9	-6
G986 r4	65	1.9	11	G995 r23 sl3	197	1.6	-2	G995 r23 sl10	153	0.8	-6
G986 r4	69	1.5	13	G995 r23 sl4	153	0.7	-3	G995 r23 sl10	161	0.8	-6
G986 r4	74	1.3	10	G955 r23 sl4	156	0.7	-4	G995 r23 sl10	163	0.8	-6
G986 r4	76	0.7	-16	G955 r23 sl4	159	0.9	-2	G995 r23 sl10	201	0.7	-2
G963 r5	172	1.0	-10	G995 r23 sl4	177	1.6	3	G995 r23 sl11	153	0.8	-6
G963 r5	184	1.5	4	G995 r23 sl4	184	1.8	3	G995 r23 sl11	155	0.7	-7
G963 r5	190	0.7	-1	G995 r23 sl4	189	1.8	1	G995 r23 sl11	161	0.9	-5
G963 r5	192	0.9	-24	G995 r23 sl4	191	1.3	-2	G995 r23 sl11	165	0.9	-5
G959 r12	122	0.8	-6	G995 r23 sl5	157	0.8	-1	G995 r23 sl12	162	0.8	-8
G959 r12	133	0.8	-8	G995 r23 sl5	159	0.8	-7				
G959 r12	138	0.9	-7	G995 r23 sl5	164	1.0	-4	G996 r8 sl5	88	0.9	-14
G959 r12	146	0.9	-6	G995 r23 sl5	166	0.8	-6	G996 r8 sl5	94	1.4	-10
G959 r32	100	0.9	-5	G995 r23 sl5	171	2.5	4	G996 r8 sl6	86	1.1	-12
G959 r32	107	0.9	-6	G995 r23 sl5	174	2.1	2	G996 r8 sl6	90	1.1	-11
G959 r32	115	1.6	9	G995 r23 sl5	177	1.6	2	G996 r8 sl6	94	1.0	-9
G959 r32	122	1.6	16	G995 r23 sl5	180	2.4	2	G996 r8 sl6	103	1.2	-16
G959 r32	128	1.6	12	G995 r23 sl5	185	2.9	0	G996 r8 sl7	86	1.1	-11
G959 r32	144	no BF/2 data see text		G995 r23 sl5	187	2.8	1	G996 r8 sl7	93	1.7	8
G750 r5	225	0.9	-4	G995 r23 sl6	157	0.8	-6	G996 r8 sl7	96	1.9	4
G750 r5	230	0.9	-3	G995 r23 sl6	162	1.0	-4	G996 r8 sl7	104	0.8	-21
G750 r5	233	0.9	-3	G995 r23 sl6	168	2.0	3	G996 r8 sl8	80	0.9	-14
G750 r5	242	1.7	10	G995 r23 sl6	172	2.3	3	G996 r8 sl8	84	1.2	-11
G750 r5	247	1.6	12	G995 r23 sl6	176	2.2	3	G996 r8 sl8	87	1.3	-9
G750 r5	250	1.7	12	G995 r23 sl6	179	2.0	3	G996 r8 sl8	95	2.4	no 70 dB BF data
G750 r5	255	1.7	13	G995 r23 sl6	183	2.2	3	G996 r8 sl9	81	1.2	-12
G750 r5	279	0.8	1	G995 r23 sl6	185	2.1	4	G996 r8 sl9	86	1.0	-12
G750 r5	285	0.7	0	G995 r23 sl7	153	0.9	-7	G996 r8 sl9	107	2.8	-8
				G995 r23 sl7	155	0.9	-6	G996 r8 sl10	79	1.1	-11
G750 r12	208	0.9	-5	G995 r23 sl7	159	0.8	-7	G996 r8 sl10	82	1.1	-12
G750 r12	211	1.0	-4	G995 r23 sl7	161	0.8	-6	G996 r8 sl10	84	1.1	-11
G750 r12	221	0.9	-4	G995 r23 sl7	172	1.4	0	G996 r8 sl10	87	1.2	-12
G750 r12	229	1.0	-6	G995 r23 sl7	200	1.2	-3	G996 r8 sl11	84	1.1	-11
G750 r12	235	0.8	-5	G995 r23 sl8	151	0.9	-7	G996 r8 sl11	87	1.1	-12
G750 r12	241	0.9	-4	G995 r23 sl8	154	0.8	-6	G996 r8 sl11	98	1.3	-6

(*continued on next page*)

Table 1 (*continued*)

G750 r12	247	0.6	-4	G995 r23 sl8	159	0.8	-6	G996 r8 sl12	81	0.9	-13
G750 r12	259	0.9	2	G995 r23 sl8	163	0.9	-5	G996 r8 sl12	85	1.0	-13
G750 r12	265	0.6	3	G995 r23 sl8	173	0.9	-6	G996 r8 sl12	89	1.0	-13
				G995 r23 sl8	176	1.1	-1	G996 r8 sl13	83	1.1	-11
G995 r23 sl1	156	1.2	-4	G995 r23 sl8	182	0.9	-6	G996 r8 sl13	86	1.1	-12
G995 r23 sl1	161	0.9	-4	G995 r23 sl8	184	1.4	-2	G996 r8 sl13	88	0.7	-13
G995 r23 sl2	159	0.8	-3	G995 r23 sl8	188	0.7	-1	G996 r8 sl13	92	1.1	-11
G995 r23 sl2	162	1.1	0	G995 r23 sl9	148	0.9	-6	G996 r8 sl14	84	1.0	-12
G995 r23 sl2	165	1.3	3	G995 r23 sl9	153	0.8	-6	G996 r8 sl14	93	1.4	-12
				G995 r23 sl9	160	0.8	-6	G996 r8 sl15	86	1.1	-8

that were negative or zero (BF gain $\geq$ BF/2 gain at 70 dB SPL), as expected based on the description just above. There were 36 *GR1* values of 1.4 and above, and of these 30 (83 %) had *GR2* values that were positive or zero (BF gain $\leq$ BF/2 gain at 70 dB SPL). As stated above, *GR2* was defined to reconcile cases in which a *GR1* value was ambiguous, and these cases are noted when describing the results. In the figures *GR1* values of 0.6 to 0.9 are colored dark blue and *GR1* values of 1 to 1.3 are colored blue. *GR1* values 1.4 to 1.7 are colored purple, 1.8 to 2.2 pink, and 2.2 and greater red. *GR2(dB)* values are in the table and are noted in the text and figures when addressing ambiguity.

DPOAE: As a monitor of cochlear condition, two-tone 2f1-f2 distortion product otoacoustic emissions (DPOAEs) were measured at the beginning of the experiment and at several time points during the experiment. f2 and f1 are the frequencies of the two tones. The DPOAEs were evoked by two simultaneously presented tones with a fixed ratio f2/f1 = 1.2 and equal levels of 50 or 70 dB SPL, presented for 1 s. The DPOAE responses typically stayed steady over hours of data collection. Initial DPOAE responses are shown in Fig. 3. In experiment 959, a cochleostomy was made prior to the DPOAE measurement, which might have produced the relatively low responses above 30 kHz, and the dip close to 20 kHz. In this experiment intracochlear motion responses were measured in the 20–25 kHz BF region in this cochlea, where the DPOAE levels were nearly within the normal range. The DPOAE responses in Fig. 3 are consistent with response levels in previous studies, for example Dong and Olson (2008).

4. Results

4.1. Introductory comparison of multitone and single-tone responses

Fig. 4 contrasts multitone and single-tone motion responses; its purpose is to demonstrate that the sub-BF nonlinearity that clearly indicates sub-BF activity is exposed at moderate SPL with multitone stimuli. In contrast, with single-tone stimuli, sub-BF nonlinearity emerges only at relatively high SPL. Fig. 4 shows frequency response gains at the BM (Fig. 4A–C) and the OHC\DC region (Fig. 4D–F) with single-tone (Fig. 4A & D) and multitone (Fig. 4B & E) stimuli. Responses are shown to stimuli spanning 45 to 95 dB SPL in the single-tone measurements, and 40 to 80 dB SPL in the multitone measurements. The BF was ~ 30 kHz; all responses within the BF peak were compressively nonlinear. At the BM, for both single and multitone stimuli, all gains were equal at frequencies below 20 kHz. These responses are considered passive; they are as they would be without activity. At the BM the 95 dB SPL single-tone gains and 80 dB SPL multitone gains were identical through the full frequency range, including the BF (comparison in Fig. 4C). These responses can also be considered passive; in this case the passive responses to sound have dominated active contributions, which have saturated at a level that makes them insignificant (distortion, not discussed here, would still be present).

In the OHC\DC-region, the single-tone responses (Fig. 4D) scaled linearly up to 75 dB SPL at frequencies below 15 kHz, whereas the multitone responses (Fig. 4E) already showed sub-BF nonlinear scaling at 53 dB SPL. The dashed lines in Fig. 4F show single, multitone comparisons, and the dotted lines in Fig. 4A & B show OHC\DC to BM comparisons, and support findings from previous studies of BM motion and OHC current. These observations can be summed up as: Multitone stimuli have overall higher sound level than their single-tone counterparts and thus produce saturation at lower levels (Fallah et al., 2019; Versteegh and van der Heijden, 2012). Multitone stimuli were used in what follows.

4.2. Results to illustrate intra-organ spatial and frequency dependence of cochlear activity

The remainder of the results section consists of examples of motion measurements, chosen to illustrate regional differences in sub-BF activity. Motion is reported at basal locations directly adjacent to the round window, with a view that is approximately transverse (~45–50 kHz BF place) and at more apical locations accessed by viewing down the cochlear spiral, at the ~ 23–32 kHz place. This optical axis contains substantial longitudinal and transverse components. One data set is included that was taken through a cochleostomy, affording a nearly transverse view at the ~ 23 kHz place. We evaluate the regional differences in sub-BF activity at two BF locations, with either primarily transverse or both transverse and longitudinal components represented, to form a relatively full picture of the degree to which sub-BF activity is present in OCC responses in the base of the gerbil cochlea.

1. Optical axis in relatively transverse direction.

Fig. 5A shows motion gain data sets, Fig. 5B shows the associated A-scan and B-scan. The measurements were made through the RW opening along the dotted line in B. The positions of the measurements spanned 25 pixels, corresponding to 68 μm. Referring to the pixel locations and the A and B-scans in Fig. 5B, pixels 51,53,55 were within the BM, pixels 65 and 69 were in the OHC\DC region and 76 was within the RL-region. Pixel 74 was only 6 μm from pixel 76, and anatomically within the OHC body close to the RL. The sub-BF responses at pixels 65,69 and 74 (OHC \DC region) appear to scale nonlinearly and are elevated relative to those at pixels 51–55 (BM), and pixel 76 (RL region). The BF peak in the OHC\DC region was apparent at 60 dB SPL but not at higher SPL, while at the BM and RL region the BF peak was apparent up to 70 dB SPL. The RL region motion (pixel 76) was like the BM in lacking significant sub-BF nonlinearity, but also showed differences — it was larger than BM motion in the BF peak, and smaller than BM motion at lower frequencies. Some oddities of the data are the amplitude trough at high SPL in the

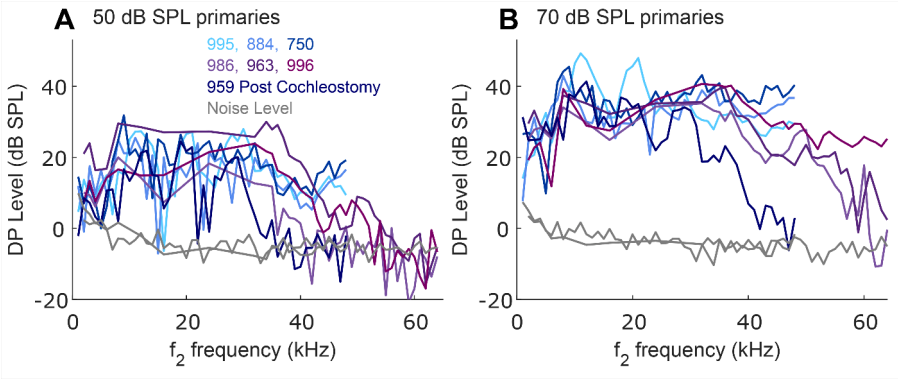

Fig. 3. DPOAE responses from the experiments in this report, measured after opening the bulla. A. 50 dB SPL primaries B. 70 dB SPL primaries. The different colors correspond to different experiments, listed in the legend in (A). Blues are experiments with motion measured in turn 1, part way down the cochlear spiral and purples from the hook region. One noise floor is shown for each type of experiment, and the noise levels were consistent across experiments. The DPOAEs were measured through f2 values of 64 or 48 kHz. A cochleostomy had been made in cochlea 959.

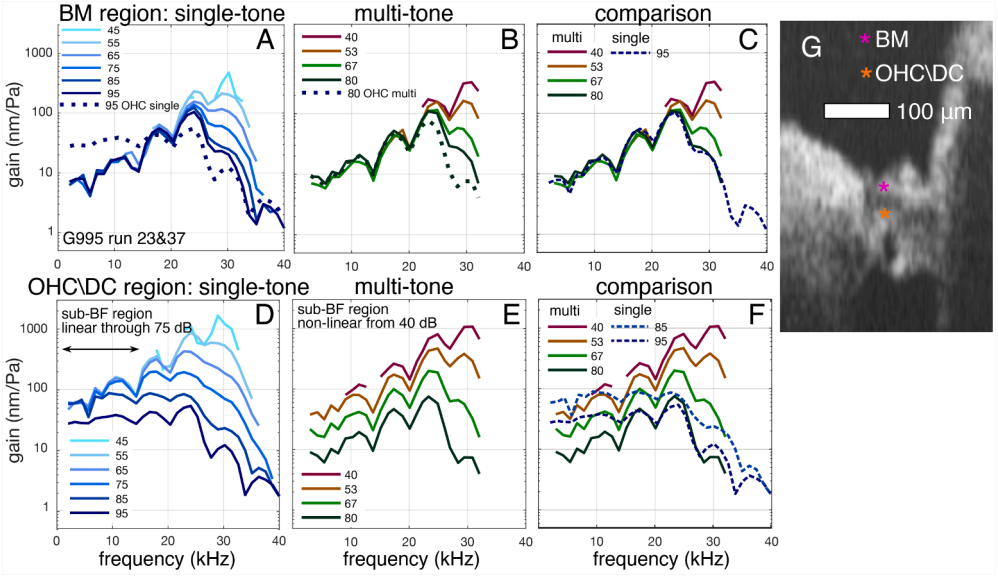

Fig. 4. A–C. BM responses to (A) single and (B) multitone stimuli with comparison in (C). D–F. OHC\DC responses to (D) single and (E) multitone stimuli with comparison in (F). G. B-scan showing locations of displayed motion responses. Responses are normalized to EC pressure as gains, so nonlinearity is apparent when curves at different stimulation levels do not overlap. Data were taken through the gerbil RW, with the optical axis aimed apically to reach the ~ 30 kHz BF location. The optical axis had longitudinal, radial and transverse components of 0.85, 0.24, 0.47. The multitone stimuli comprised 25 frequency components, spanning 3 to 32 kHz. Gerbil 995 runs 23&37.

OHC\DC region (pixels 65,69,74), occurring along with a phase shift. (The word "trough" is used rather than "notch" because the reduction can span a relatively wide frequency range.) The complex difference analysis in the discussion will explore this behavior.

Fig. 5D shows the phases from the three different anatomical locations, pixels 53 (BM), 69 (OHC\DC) and 76 (RL region), at 70 dB SPL, and phase differences are shown in Fig. 5E. 70 dB SPL data are shown because there was not much variation between SPLs except at 80 dB SPL and the 70 dB SPL data are out of the noise through a relatively wide frequency range. In Fig. 5D, 80 dB SPL OHC\DC region phase is included and shows that at frequencies above the phase shift, the OHC\DC phase was almost in line with the BM and RL phases. The RL region and BM phases were relatively similar but not identical, with the RL region phase leading the BM phase by a value that increased from ~ 0 to ~ 0.15 cycle from 18 to 35 kHz. The OHC\DC region was close to half a cycle out of phase with the RL region (varying between 0.4 and 0.6 cycles difference) from 20 to 40 kHz.

Fig. 5C is a table of metrics as defined and described in the methods. *GR1*, the ratio of gains at 70 and 80 dB SPL, found at BF/2, is a direct measure of sub-BF nonlinearity. If *GR1*>1.3, sub-BF activity is considered present. *GR2(dB)* is the dB value of the ratio of the gain at BF/2 to the gain at BF, measured at 70 dB SPL. Positive *GR2(dB)* values suggest sub-BF activity. Pixels 51, 53, 55, 60, 76 have *GR1* values ranging from 0.7 to 1.3 and their negative *GR2* values are consistent with lack of sub-BF activity. The *GR1* values of pixels 65 and 69 indicate sub-BF nonlinearity, and their positive *GR2(dB)* values are consistent. Pixel 74 was ambiguous by the two metrics, with a *GR1* value of 1.3, and a *GR2(dB)* value of +10. Observing the full frequency response at pixel 74, the *GR1* value was reduced by a ripple in the response at BF/2, and the large positive *GR2(dB)* value indicating sub-BF activity is more robust.

Fig. 6 is another measurement made through the RW with the optical axis nearly transverse. It reinforces observations of Fig. 5: sub-BF near-linearity in the BM and RL regions (Fig. 6A & C), sub-BF nonlinearity in the OHC\DC region (Fig. 6B) along with an amplitude trough and phase shift at high SPL (80 dB SPL). The RL region motion was larger than BM motion in the peak, and smaller at lower frequencies. The phase differences shown in Fig. 6D & E are like those of Fig. 5D & E, with a nearly

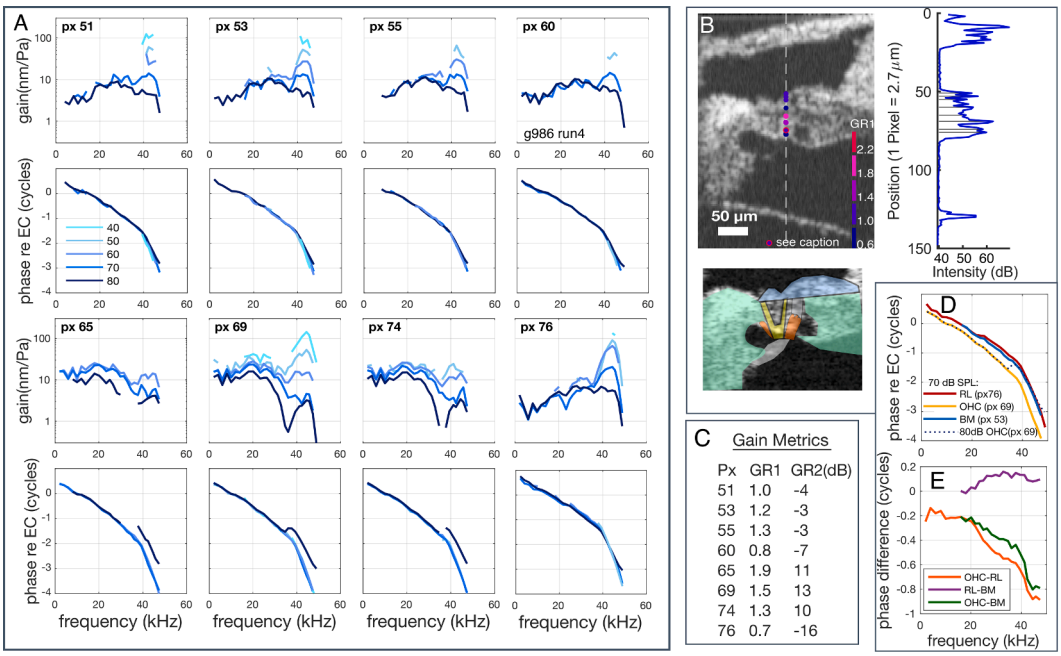

Fig. 5. A. Results from eight positions along one axial scan (A-scan). The top panels show gain (displacement/EC pressure), bottom panels show phase relative to ear canal (EC) pressure. B. B-scan and A-scan for this data set. The dashed line in the B-scan is the displacement measurement axis, with the color-coded dots indicating the GR1 values. The blue dot with red surround is a point (px 74) in which the GR1 and GR2 values were not aligned (further discussion in text). The A-scan is registered to the B-scan to approximately identify the anatomical locations of measurement. The lower B-scan is anatomically color-coded as in Fig. 1. C. Gain metrics. D. Phases measured at 70 dB SPL from three representative locations. E. Phase differences. The multitone stimuli comprised 35 frequency components, spanning 2 to 60 kHz. The optical axis longitudinal, radial and transverse components were −0.48, −0.35, 0.8. Gerbil 986 run 4 BF 44 kHz.

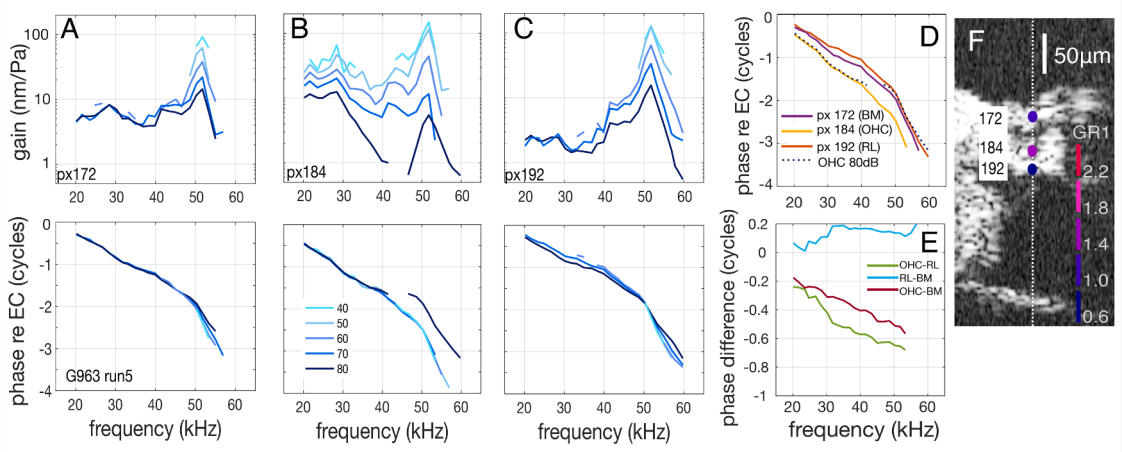

Fig. 6. Another example of transverse data. A-C are gain and phase responses at the three pixels indicated in the B-scan in F, with the color-coded dots in F indicating GR1 values. D and E show phase comparisons. Gain metrics: px172 GR1=1, GR2(dB)=−10; px184 GR1=1.5, GR2(dB)=4, px192 GR1=0.9, GR2(dB)=−24. The multitone stimuli comprised 20 frequency components, spanning 20 to 60 kHz. Gerbil 963 run 5. BF= 52 kHz.

half cycle difference between the OHC\DC region and the RL region from 30 to 50 kHz, the RL region leading the BM by up to 0.2 cycles, and the 80 dB OHC\DC-region phase lifting to join the BM and RL region phase at frequencies above those of the trough.

In the preparation of Fig. 7, also measured with the transverse optical axis, a mapping of transverse motion was performed, with OCC regions medial and lateral to the OHC region also observed. Slices and pixel values are indicated, and their locations noted in the B-scan (Fig. 7B). Three points, slice 7 pixels 93 & 96, slice 8 pixel 95, showed sub-BF nonlinearity based on the metrics, and are in the OHC\DC region of the B-scan. These pixels also contained phase offsets relative to BM and a phase lift at 80 dB SPL to join the BM-like phase (Fig. 7C), as in the OHC \DC region of Figs. 5 & 6. The responses at other points were generally approximately linear sub-BF, but with some outliers. For example, slice 9 pixel 107, shows sub-BF nonlinearity, but does not show the high SPL amplitude trough of the OHC\DC regions points, and the metrics of this point (*GR1=2.8, GR2(dB)=−8*) are ambiguous. Although it lacked the 80 dB phase lift, at other SPLs the phase of slice 9 pixel 107 is like that of the OHC\DC points (slice 7 pixel 93,96 and slice 8 pixel 95). From the B-scan, the location of slice 9 pixel 107 is just below the outer tunnel within the tectal cells that join the lateral OCC to the RL, and its motion might be heavily influenced by fluid motion. Adjacent points in the RL region (slice 6 pixel 103 and slice 7 pixel 104) lacked substantial sub-BF nonlinearity, with phases close to the BM phase (Fig. 7C). Slice 6 pixel 94 is another unusual point, sub-BF linear by both metrics and by shape, but with relatively high gain values. In the B-scan this point is in the region of the pillar cells and tunnel of Corti. From slice 9 through slice 15, a region spanning 70 µm laterally, all points except the unusual slice

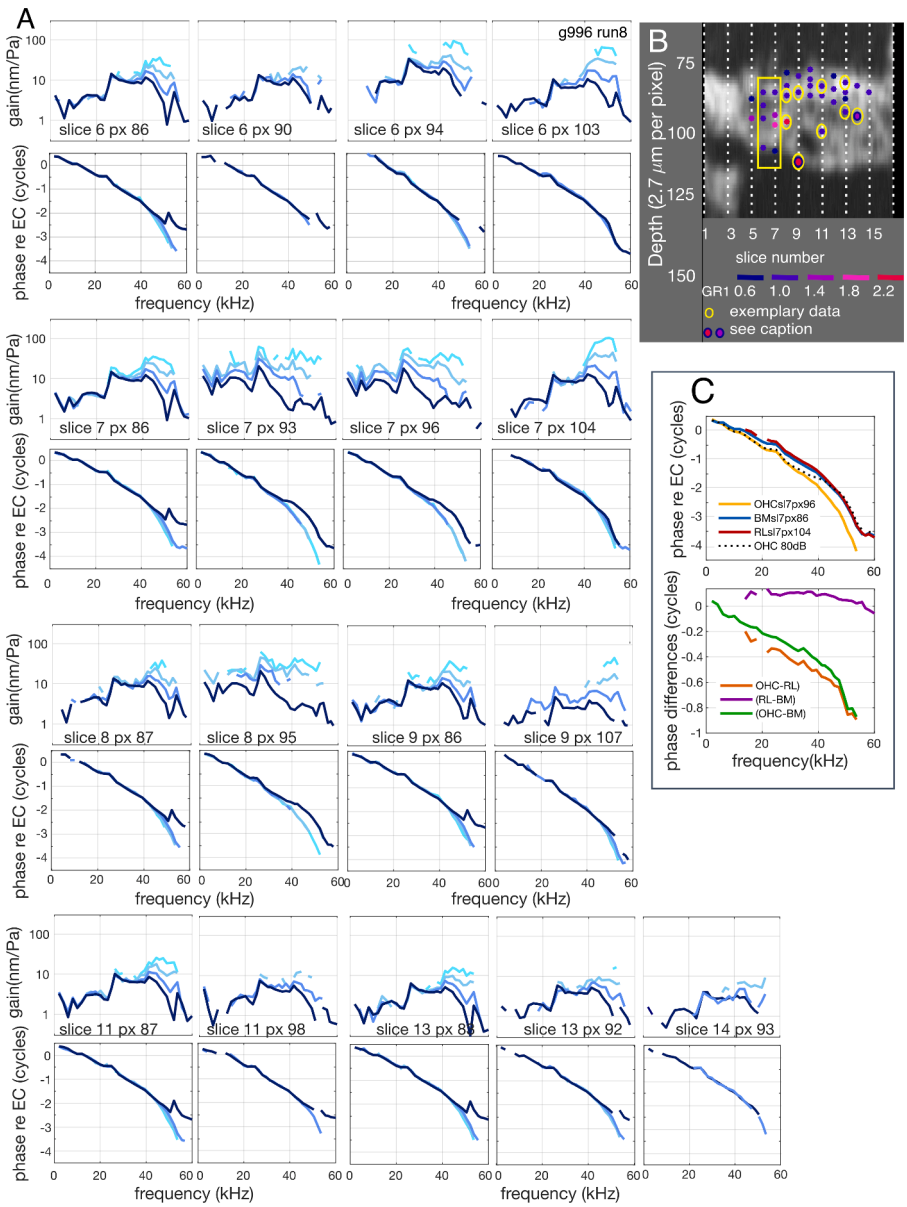

Fig. 7. Response map. A. Responses at locations indicated in the B-scan in (B). The yellow rectangle and circles identify locations where exemplary data are shown. Multitone stimuli were applied at 50, 60, 70, 80 dB SPL (lighter to darker blue). In (A) the top panels show gain (displacement/EC pressure), bottom panels show phase relative to EC pressure. The lines in the B-scan are separated by 20 μm. The color-coded dots code GR1 values. The two dots with surrounding colors had non-aligned GR1 and GR2 values. Slice 9 px 107 is discussed in the text, Slice 14 px 93 had an GR1 value of 1.4 (indicating sub-BF activity), and a GR2 value of −12 (indicating lack of sub-BF activity). The GR1 value of 1.4 can be attributed to a response notch at the frequency of BF/2. When additional sub-BF frequency points are considered, this location is approximately linear sub-BF. C. Phases and phase differences from three locations in slice 7 (px 86, 96 and 104). (70 dB SPL data were used for px 86 and px 104, 60 dB SPL for px 96 to include a longer frequency range.) The multitone stimuli comprised 35 frequency components, spanning 2 to 60 kHz. Longitudinal, radial and transverse components were −0.31, −0.13, 0.94. Gerbil 996 run 8.

9 pixel 107 noted above were approximately linear sub-BF, with negative *GR2(dB)* values, and with phases close to those of the BM.

In Fig. 8 we show two data sets from the ~ 23 kHz BF location from the same cochlea. Fig. 8A–C data were taken through a cochleostomy above the stapedial artery (Fig. 2B), affording a nearly transverse view but limited to the very medial part of the OCC. These results did not include any locations with clear sub-BF nonlinearity. Locations A and B are close to or within the BM. Location C, 65 μm deeper than point A, is close to the RL region, perhaps at the radial location of an inner hair cell. The phases were quite similar across these locations.

2. Optical axis containing substantial longitudinal component.

The B-scan in Fig. 8H is distorted from the transverse-radial view (Fig. 2A) due to the longitudinal\transverse optical axis, and the most obvious landmarks are the dark regions that correspond to the outer tunnel (below purple dot) and tunnel of Corti (above-left of purple dot), which sandwich the OHC\DC region (purple dot). The motion at the BM (Fig. 8E) and ~120 μm within the OCC, in the region lateral to the outer tunnel (Fig. 8G) scaled approximately linearly sub-BF, while the OHC \DC-region motion (Fig. 8F) showed sub-BF nonlinearity. The OHC \DC region also showed an amplitude notch and phase shift at the highest SPL, but the notch and phase shift are different from those in Figs. 5–7; in Figs. 5–7 the 80 dB OHC phase shifted to join the BM phase, in Fig. 8F the OHC\DC-region phase was generally quite similar to BM phase (60 dB dotted pink line gives a direct comparison) and the notch-

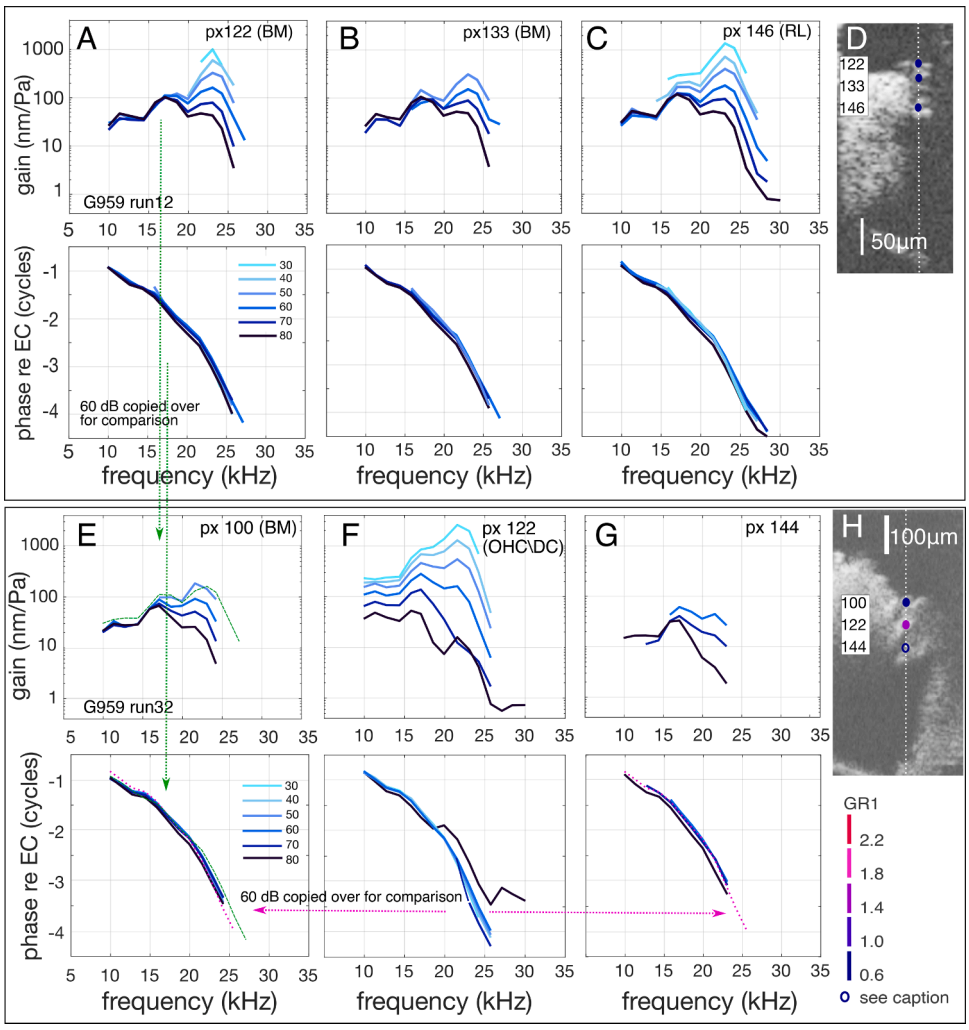

Fig. 8. E–G data were from the same cochlea as Fig. 8A–C, taken through the RW with the optical axis with a substantial longitudinal component, pointing apically to reach the same ~ 23 kHz BF location. The BM responses in Fig. 8E were like the BM responses measured through the cochleostomy, with a direct comparison of Fig. 8A included in Fig. 8E (green dashed lines). The BM is expected to move purely transversely, which would reduce the magnitude of the measured BM motion in Fig. 8E compared to Fig. 8A by the ratio of the transverse components of the optical axis in the two measurements (through-RW/through-cochleostomy). However, the Fig. 8A data were collected medial, closer to a rigid boundary, at a position that would move less than a more central radial position. Thus, there are two competing effects, and the result, with the Fig. 8A 60 dB gain line slightly above the Fig. 8E 60 dB line, is reasonable. The Fig. 8A–C data peaked at a just slightly higher BF than Fig. 8E–G, due to inexact matching of BF location.

related phase shift at 80 dB shifted the phase away from the BM phase. The amplitude notch and phase shift in Fig. 8F are likely related to the OHC\DC-region motion being nearly perpendicular to the optical axis when the optical axis is substantially longitudinal (Frost et al., 2022, 2023a, 2023b). At frequencies below 15 kHz the OHC\DC region phase led the BM slightly (Fig. 8E).

Fig. 9 is another example of data taken with the optical axis pointing apically down the cochlea to reach the ~ 25 kHz location. This preparation had relatively high reflectivity deep into the OCC. The left A-scan spanned the fluid regions that flank the OHCs (Fig. 9H) and the OHC\DC region motion showed sub-BF nonlinearity (Fig. 9B), but a deeper location seemingly close to the RL (Fig. 9C) lacked sub-BF nonlinearity. At frequencies below 10 kHz the OHC\DC region phase led the BM and RL-region slightly (Fig. 9A & C). Locations probed in a second A-scan ~ 100 µm lateral (Fig. 9D–G) lacked significant sub-BF nonlinearity.

The measurements in Fig. 10 were made with the optical axis substantially longitudinal to reach the ~ 31 kHz BF location. Motion gain data are shown in the plots to the left of the orienting B-scan and a subset of phase data is in Fig. 10C. The dark fluid-filled spaces in the B-scan that flank the OHC\DC region were used to identify that region. Three exemplary data sets possessed clear sub-BF nonlinearity (slice 4 pixel 184, slice 6 pixel 179, slice 7 pixel 172). Slice 3 pixel 197 was ambiguous and slice 4 pixel 191 was linear sub-BF based on the metrics, but when considering frequency points near BF/2, a degree of sub-BF nonlinearity is present. These two positions appear to be close to the RL, but the longitudinal view obscures the cross-sectional anatomy too much to know. From slice 8 through slice 12, spanning ~ 50 µm laterally, all points were approximately linear sub-BF. (Slice 8 pixel 184 had non-aligning metrics, but is approximately linear sub-BF when frequency points near BF/2 are considered.) The phase responses in Fig. 10C show the same slight lead of OHC/DC region compared to BM (upper panel) and RL-region (lower panel) that was observed in Figs. 8E–G & 9.

It is noteworthy that the phase of OHC/DC relative to BM motion was a lag when measured in the nearly transverse direction (Figs. 5–7), and a lead when measured with the substantially longitudinal view (Figs. 8E–G,–10). Such angle-dependent phases are attributable to the 3-dimensional nature of the OHC\DC region motion (Cooper et al., 2018; Frost et al., 2023a, 2023b).

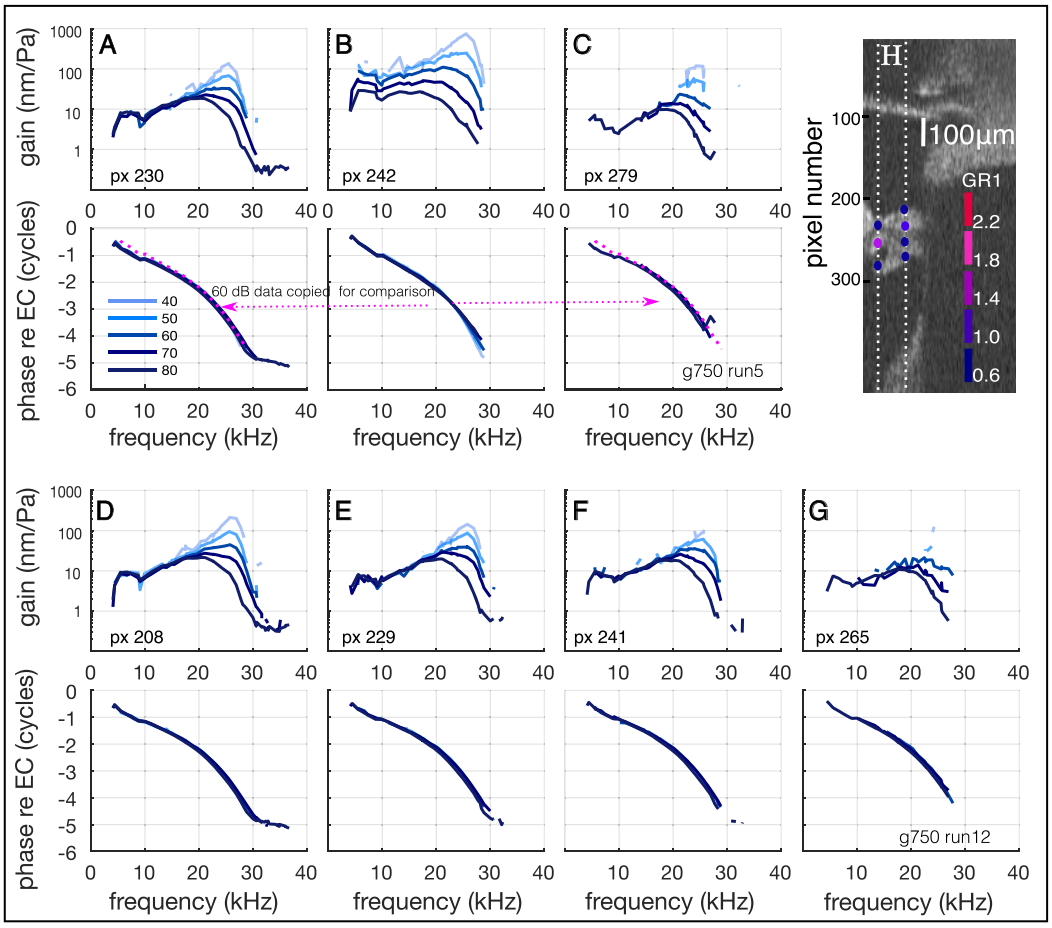

Fig. 9. Another example in which data were taken through the RW opening, with a substantial longitudinal component to the optical axis. Responses were measured over two A-scans, indicated in the color-coded dots in the B-scan in H. A-C are from the left A-scan, D–G are from the right A-scan. Gerbil 750, runs 5&12. Metrics: run 5 px 230 GR1=0.9, GR2(dB)=−3; run 5 px 242 GR1=1.7, GR2(dB)=10; run 5 px 279 GR1=0.8, GR2(dB)=1. run 12 px 208 GR1= 0.9, GR2(dB)= −5; run 12 px 229 GR1= 1.0, GR2(dB)= −6; run 12 px 241 GR1= 0.9, GR2(dB)= −4; run 12 px 265 GR1= 0.6, GR2(dB)= 3.

5. Discussion

5.1. Regional variations in sub-BF nonlinearity, and comparisons with previous observations

The measurements of Figs. 5–7 were made through the RW with a nearly transverse approach. The OHC/DC region showed substantial sub-BF nonlinearity, whereas RL and BM regions lacked significant sub-BF nonlinearity. This transverse approach was also used in Cho and Puria (2022). They used single-tone stimuli and the presence of sub-BF nonlinearity was not obvious pre-mortem in any region (review Fig. 4), but sub-BF activity was observed *via post-mortem* reduction in motion in the OHC/DC region. In the RL region and BM, sub-BF motion was not reduced post-mortem. Thus, the observations from both labs indicate absence of sub-BF activity in the RL region. It is notable however, that Cho and Puria observed changes in the sub-BF phase response of the RL region post-mortem.

The measurements of Figs. 8E–G–10 were made with an approach through the RW opening and angling longitudinally to reach relatively apical locations. Substantial sub-BF nonlinearity was present in the OHC/DC region, with insignificant sub-BF nonlinearity at the BM. Because of the steep longitudinal optical angle, the RL region could not be clearly identified in the B-scans. However, the locations represented in Figs. 8G and 9C were close to or within the RL region and these results were approximately linear sub-BF. The longitudinal viewing angle was employed in several of our previous studies, which emphasized the BM and OHC\DC regions (Strimbu et al., 2020, 2022; Fallah et al., 2019; Frost et al., 2022, 2023a, 2023b) and the results presented here agree with those previous results and with the earlier results of Cooper et al. (2018).

Fig. 8A–C reported observations made through a cochleostomy, to make approximately transverse measurements at the ~ 25 kHz location. The view was limited to the medial OCC and did not include the OHC region. Measurements were made at the BM and a deeper point that was likely close to the RL and pillar cells' heads. Sub-BF responses were approximately linear at all positions. It is not surprising that this medial section of the RL would move similarly to the BM, given the stiff rods of the pillar cells (Olson and Mountain, 1994; Zetes et al., 2012; Cho and Puria, 2022). In Fig. 8E–G the same BF frequency region in the same preparation was observed with the relatively longitudinal view, *via* the RW. The BM motion, amplitude and phase, was directly compared from the two viewing angles and the overall similarity supports the view that the BM moves transversely, with motion that is similar, simply scaled, at different viewing angles (Frost et al., 2023a, 2023b; Cooper et al., 2018).

He et al. made measurements at the ~ 25 kHz BF location both through the RW (He et al., 2018) and through a cochleostomy (He et al., 2022a). In the latter case, they displaced the stapedial artery, which afforded a more complete view of the OCC than we had in Fig. 8A–C. Their system did not include B-scan imaging, and the RL and BM were identified as reflective surfaces with a reasonable separation distance. The region they identified as the RL exhibited sub-BF activity: nonlinearity and postmortem reductions in motion. Our observations seem to conflict with those. However, as noted above, our measurements from the ~ 25 kHz BF place did not convincingly identify the RL region above

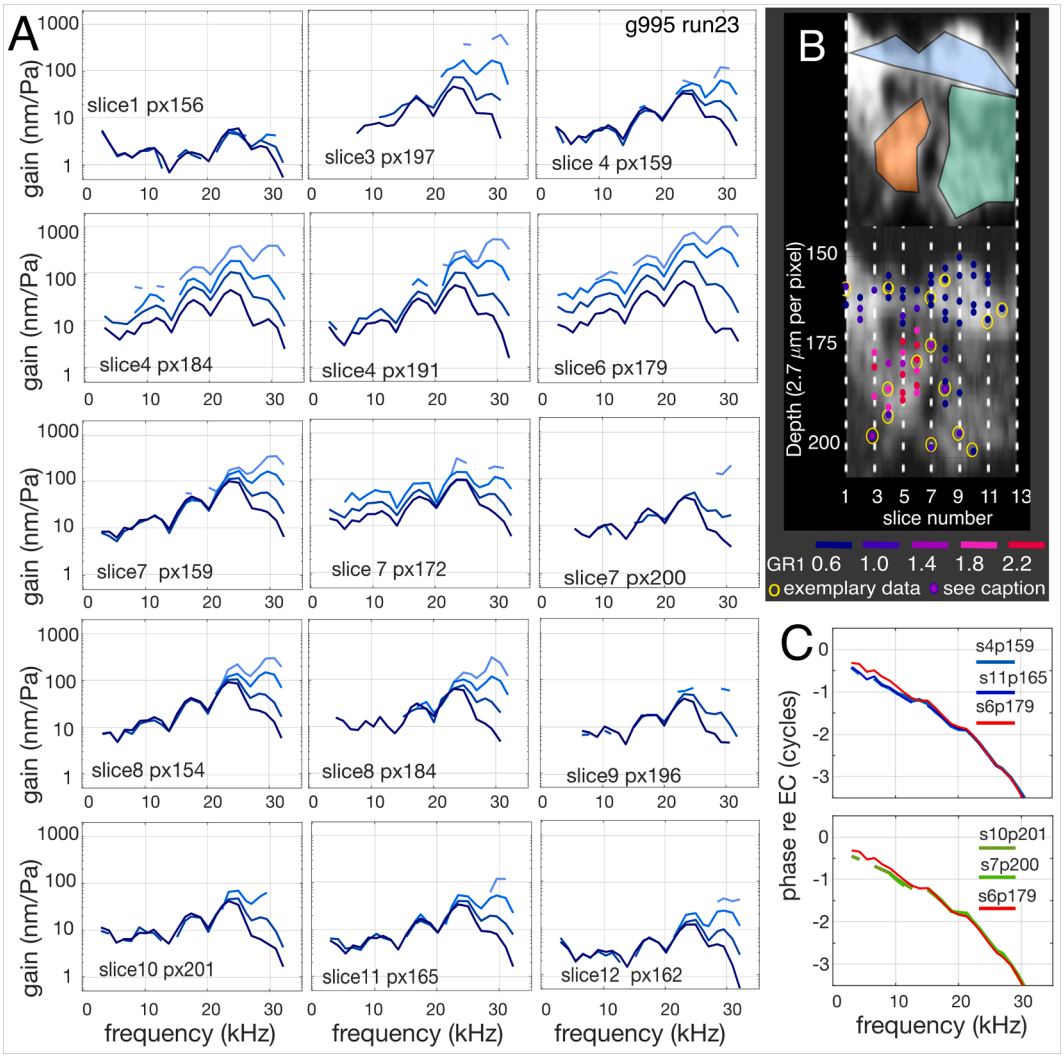

Fig. 10. Response map. A. Gain responses at locations color-coded by GR1 value in the B-scan in (B). The dashed lines in the B-scan are separated by 20 μm. Multitone stimuli were applied at 40, 53, 67, 80 dB SPL (lighter to darker blue). The yellow circles identify locations where exemplary data are shown. Location slice 3, px 197 (GR1,GR2 = 1.6,−2) and slice 8 px 184 (GR1,GR2= 1.4, −2) had non-aligning GR1 and GR2 values, so are circled with blue to indicate negative GR2 values. C. (Top) Phase data from the BM region are compared to a phase from the OHC\DC region, slice 6, px 179. (Bottom) Phase data from two locations in the lateral region are compared to a phase from the OHC\DC region, slice 6, px 179. Optical axis longitudinal, radial and transverse components were 0.85, 0.24, 0.47. Gerbil 995 run 23. Gain metrics are in Table 1.

OHCs, either because of the viewing axis, or limited radial view. Further studies are needed to reconcile these results.

Motion from the lateral region of the OCC was recorded from three preparations and both viewing angles, in Figs. 7 (G996), 9 (G750) and 10 (G995). Lateral slices that included both BM and deeper points were: G996: slice 11,13,14; G750: run12; G995: slice 8,9,10. From the B-scans and Table 1, these slices included 22 points within the BM and 16 points within the lateral cells. The means and standard deviations of the *GR1* values in the two regions were, BM: mean = 0.91, standard deviation = 0.11; lateral: mean = 0.93, standard deviation = 0.26. Both these ranges include the value *GR1* = 1, corresponding to perfect linearity at BF/2. Calculating a two-tailed Student's t-test between the BM and lateral regions, the P value was 0.76, which indicates that the *GR1* metric, representing sub-BF linearity, was not statistically different in the BM and lateral regions. To our knowledge, the lateral region of the OCC in the cochlear base has not been evaluated for sub-BF activity previously, but a regional comparison in the gerbil apex (~ 3 kHz BF) has been made (Meenderink et al., 2022). In the gerbil apex, nonlinearity (observed at BF/2 with multitone stimulation) extended through all spatial regions of the OCC, even the BM. This is different than the basal observations. A similarity between the basal and apical locations is that the degree of sub-BF nonlinearity in the apex was substantially larger in the OHC region than in the TM, BM, and lateral regions of the OCC.

5.2. *OHC-region behavior when optical axis is relatively transverse — complex differences to find internal motion*

The motion measured along an approximately transverse optical axis (Figs. 5–7) possessed magnitude troughs and associated phase shifts in the OHC\DC region. These characteristics suggest that the measured transverse OHC\DC-region motion can be considered as a sum of an internal OHC\DC motion and the motion of the BM. With its set of tightly packed, radially-oriented collagen fibers (de Sousa Lobo Querido et al., 2023; Dreiling et al., 2002), the BM is the major supporting structure of the OCC and as noted above, its motion is primarily transverse. Taking the complex difference, OHC\DC-region minus BM motion, provides an estimate of the internal transverse motion of the OHC \DC-region. This analysis is illustrated in the cartoon of Fig. 11, and the analysis was done for the data of Figs. 5–7 and shown in Fig. 12. In Figs. 11 & 12, BM motion is blue, OHC\DC-region motion is red, and

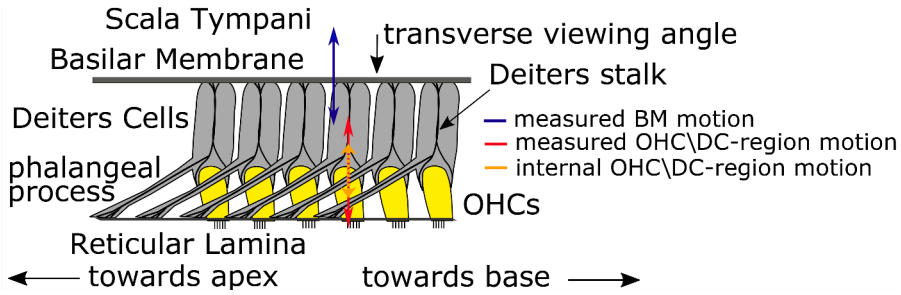

Fig. 11. Longitudinal-transverse cartoon of the OCC from the basilar membrane to the reticular lamina. The motion directly measured in the OHC\DC region (red) can be considered as resulting from the sum of the motion of the BM (blue) and the internal motion of the OHC\DC region (gold). The Deiters stalk and phalangeal processes of the Deiters cells tether the basilar membrane to the reticular lamina.

their complex difference is gold. Because the BM and OHC\DC-region motions can be nearly out of phase, the magnitude of their difference was often larger than the magnitudes of the OHC\DC region and BM motion. This is particularly evident in the BF peak in the gold curves in Fig. 12A at 50–60 dB SPL, in Fig. 12B at 50–70 dB SPL and Fig. 12C at 50–60 dB SPL. The (red) OHC\DC magnitude trough is either absent or reduced in the calculated internal motion (gold), and the phase shift observed in the measured OHC\DC motion is not present in the internal motion. In the 80 dB curves of Fig. 12A–C the reason for the trough in measured OHC\DC-region motion (red) is easily traced to the equal amplitudes and half cycle phase differences of the blue and gold curves of BM and internal OHC\DC-region motion. Thus, the results of the complex difference analysis clarified the amplitude troughs and phase shifts of the measured motion. The results also show that the size of the internal OHC\DC motion is maintained relatively high through a higher frequency than the directly measured OHC\DC motion.

At the far right of the panel sets is the phase of the internal OHC\DC motion relative to the BM. This phase is similar across sound levels (50–80 dB SPL) and preparations. The phase is close to zero at the lowest frequencies and decreases generally smoothly and steadily to a value of −0.5 cycles just below BF and continues decreasing to a value of ~ −0.6 cycles. The significance of this internal OHC\DC motion, moving largely in the opposite direction relative to the motion of the BM, is not known. It is possible that it is simply an epiphenomenon of the active process. Conversely, fluid moving to accommodate the internal motion may be critical to the longitudinal flow of energy towards the best place. Several recent cochlear models have explored the role of active fluid flow in frequency tuning (Altoè et al., 2022; Guinan, 2022; He et al., 2022b).

5.3. Significance for hair cell excitation

Neural tuning is more similar to BM than OHC\DC motion tuning (Narayan et al., 1998; Cooper et al., 2018; Meenderink et al., 2022). Hair cells are stimulated by the pivoting motion of stereocilia, which in Fig. 2A stand below the RL and insert (OHCs) or nearly insert (IHCs) into the TM (Lim, 1972). In the results of this study, the RL region lacked significant sub-BF activity and the RL tuning in evidence in the transverse measurements (Fig. 5 pixel 76, Fig. 6C and Fig. 7 slice 7 pixel 104) was at least as well tuned as the adjacent BM, with a higher BF peak, consistent with the observations of Cho and Puria (2022). Based on these observations, it seems likely that in the healthy cochlear base, hair cell stereocilia are not stimulated by the sub-BF motion that is present in the OHC\DC region. In damaged cochleae, high-frequency auditory neurons can become hyper-sensitive to sub-BF tones and contain temporal firing patterns including phase locking that are not present in healthy high-frequency auditory neurons (Versnel et al., 1997; Kale and Heinz 2010). It is possible that in damaged cochleae, OHC sub-BF activity is less shielded from other regions of the OCC, leading to pathological auditory nerve responses. On the other hand, a presence of sub-BF activity in stereocilia stimulation could account for the finding that sub-BF responses of high-frequency auditory nerve fibers were inhibited by medial olivocochlear activity and suppressed by a low-frequency suppressor (Nam and Guinan, 2018). Thus, the literature is mixed on this question.

The measurements reported here did not include the TM, which was not reflective enough to provide the vibration responses necessary to evaluate sub-BF nonlinearity. In reports from the mouse 9 kHz BF region, with an optical axis containing radial and transverse components, the TM vibrated like the BM and not like the OHC region, in terms of nonlinearity and post-mortem responses (Dewey et al., 2018; Dewey, 2022). However, earlier results did observe sub-BF nonlinearity in the TM and RL (Lee et al., 2016). Overall, the motion in the OHC\TM\RL region is spatially varying in three dimensions, and the motion is still being ironed out.

5.4. Physical ramifications of spatially limited sub-BF activity

Nonlinear motion abutting tissue exerts nonlinear forces on that tissue. Considering Fig. 11, the internal nonlinear OHC motion will transmit nonlinear forces to the Deiters cells and RL. However, sub-BF nonlinear motion was usually absent at the RL and lateral regions of the OCC. Thus, sub-BF forces on these OCC structures must be dominated by passive forces. A primary force on the BM is the pressure on its scala tympani surface. This pressure has been measured in active cochleae and is tuned and nonlinear in the BF peak, but sub-BF is linear and passive (unchanging *post-mortem*) (Olson, 2001; Dong and Olson, 2013). The slow wave pressure on the scala media side of the OCC is theoretically equal in magnitude to the pressure in scala tympani, and opposite in phase. Pressure measured in scala media was consistent with that expectation, although the preparation was in an unavoidably damaged condition (Kale and Olson, 2015). Pressure and BM motion are partners in the cochlear traveling wave, and previous studies have reported that sub-BF activity is not transported by the wave (Dewey et al., 2019; Fallah et al., 2019; Guinan, 2022). Thus, it is reasonable that at sub-BF frequencies the pressure is a dominant force governing OCC motion.

The pillar cells and the Deiters stalk, composed of structural proteins (microtubules, actin and intermediate filaments) anchor the RL to the BM (Zetes et al., 2012; Engstrom and Wersall, 1958; Parsa et al., 2012; Zhou et al., 2022). The physical properties and orientation of these structures might constrain the RL to move more like the BM, and not like the OHCs. The phalangeal processes of the DCs course apically (Fig. 11) and as the cochlear wave travels apically, their mechanical effect will be to impose basal BM motion on the more apical RL location. Thus, in transverse measurements of the RL and BM vibration, the RL would be predicted to lead the BM. The value of the predicted phase lead depends on the traveling wave wavelength, which is ~ 0.4 mm at frequencies getting close to the BF (Ren 2002) and longer at lower frequencies. The phalangeal processes in the gerbil base span a longitudinal distance of ~ 0.08 mm (Wang et al., 2016). Thus, at frequencies approaching the BF the phalangeal processes span ~ 0.2 wavelength, corresponding to 0.2 cycle. This is close to the measured RL re BM phase lead in Figs. 5E, 6E

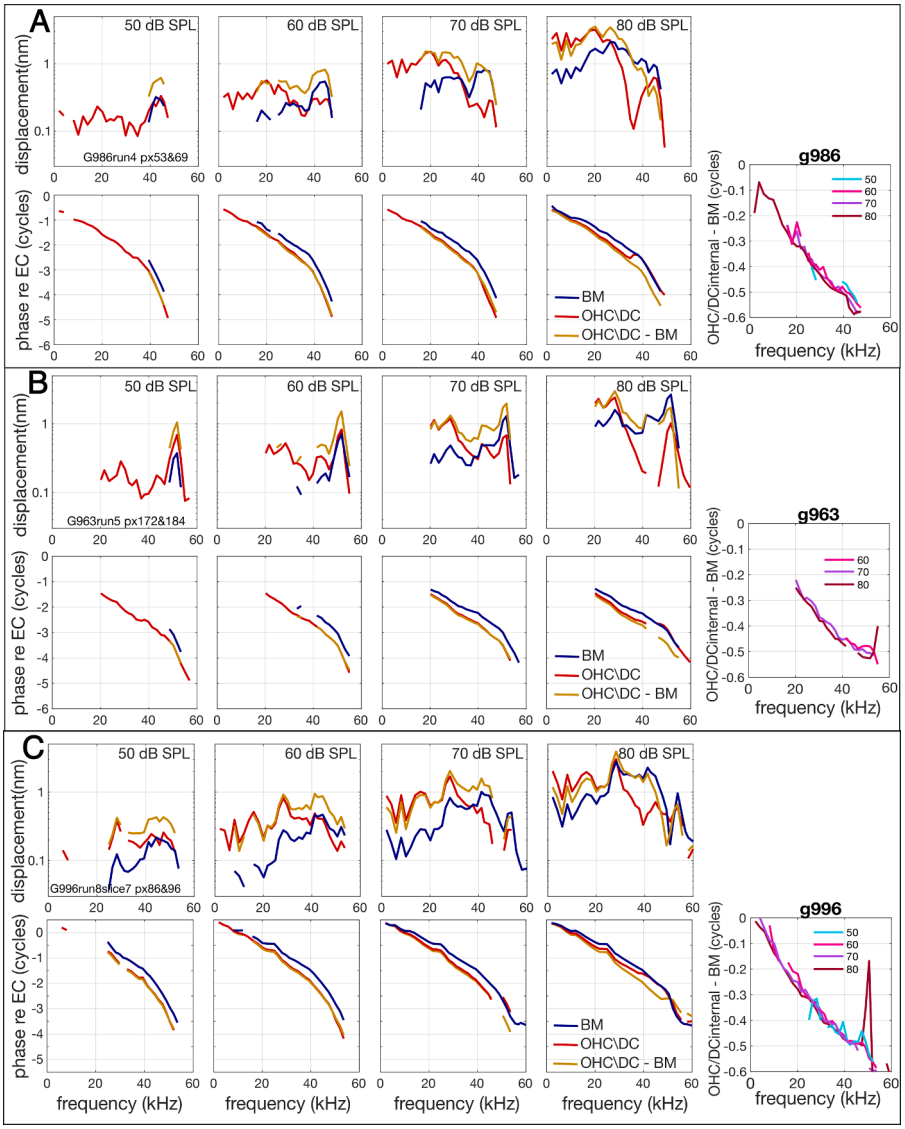

Fig. 12. Complex difference between OHC\DC region and BM responses was taken to reveal internal OHC\DC motion. In each preparation the responses going into the difference were measured along a single A-scan as in the motion data of Fig. 5 (Gerbil 986), Fig. 6 (Gerbil 963) and Fig. 7 (Gerbil 996). Results are shown in panel sets A, B, C, respectively. Each panel set has subpanels corresponding to different SPLs and within each subpanel, the OHC\DC and BM data are shown in red and blue, and the OHC-BM complex difference is shown in gold. To the far right the phase of the internal OHC\DC motion is plotted referenced to the BM motion.

and 7C. This correspondence is dimmed by the observation by Cho and Puria (2022) that the phase lead disappeared post-mortem, which would not be the case if the intracellular anchoring structures were maintained for a time after death. Nevertheless, a role for the Deiters stalks in imposing BM-like motion on the RL is possible. The pillar cells most certainly have such a role based on their significant stiffness (Olson and Mountain, 1994) and supported by recent across-RL measurements (Cho and Puria, 2022).

A central question of cochlear mechanics remains: how does the BM respond to OHC active forces only at frequencies in the BF peak, when OHC active forces are present through the full range of sub-BF frequencies? Mathematical models and concepts can replicate this phenomenon (Nankali et al., 2020; Yoon et al., 2011; De Boer and Nuttall, 2000; Altoè et al., 2022; Sisto et al., 2021; Dong and Olson, 2013) but their physiological and anatomical underpinnings remain tenuous. OCT has delivered a wealth of data regarding the coordinated responses of OHCs, supporting cells and their surrounding extracellular structures. In the current analysis, OCT observations have shown that in the cochlear base the sub-BF activity of the OHC\DC region, long known to be absent from the BM, also appears to not significantly penetrate the lateral OCC or RL regions, and this regional separation is likely essential for healthy cochlear function.

Funding

NIDCD R01 DC015362 (Elizabeth Olson PI).
NIDCD F31 DC020621 (Brian Frost PI).
Emil Capita Foundation.

CRediT authorship contribution statement

C. Elliott Strimbu: Performed experiments, Analysis, Edited paper. **Lauren A. Chiriboga:** Analysis, Edited paper. **Brian L. Frost:** Analysis, Edited paper. **Elizabeth S. Olson:** Analysis, Wrote paper.

Declaration of competing interest

The authors declare no financial interests or conflicts of interest.

Data availability

Data will be made available on request.

Acknowledgments

Funding was provided by the NIDCD grants R01 DC015362 (Elizabeth Olson PI) and F31 DC020621 (Brian Frost PI). Funding was provided by the Emil Capita Foundation. We thank the *Hearing Research* reviewers and Associate Editor for their comments and discussion.

References

Altoè, A., Dewey, J.B., Charaziak, K.K., Oghalai, J.S., Shera, C.A., 2022. Overturning the mechanisms of cochlear amplification *via* area deformations of the organ of Corti. J. Acoust. Soc. Am. 152, 2227–2239.
Cho, N.H., Puria, S., 2022. Cochlear motion across the reticular lamina implies that it is not a stiff plate. Sci. Rep. 12, 18715.
Cooper, N.P., Vavakou, A., van der Heijden, M., 2018. Vibration hotspots reveal longitudinal funneling of sound-evoked motion in the mammalian cochlea. Nat. Commun. 9 (1), 3054.
De Boer, E., Nuttall, A.L., 2000. The mechanical waveform of the basilar membrane. III: intensity effects. J. Acoust. Soc. Am. 107, 1497–1507.
de Sousa Lobo Ferreira Querido, R., Ji, X., Lakha, R., Goodyear, R.J., Richardson, G.P., Vizcarra, C.L., Olson, E.S., 2023. Visualizing collagen fibrils in the cochlea's tectorial and basilar membranes using a fluorescently labeled collagen-binding protein fragment. JARO 24, 147–157.
Dewey, J.B., Xia, A., Muller, U., Belyantseva, I.A., Applegate, B.E., Oghalai, J.S., 2018. Mammalian auditory hair cell bundle stiffness affects frequency tuning by increasing coupling along the length of the cochlea. Cell Rep. 23, 2915–2927.
Dewey, J.B., Applegate, B.E., Oghalai, J.S., 2019. Amplification and suppression of traveling waves along the mouse organ of Corti: evidence for spatial variation in the longitudinal coupling of outer hair cell-generated forces. J. Neurosci. 39, 1805–1816.
Dewey, J.B., 2022. Cubic and quadratic distortion products in vibrations of the mouse cochlear apex. JASA Express Lett. 2 (11), 114402.
Dong, W., Olson, E.S., 2008. Supporting evidence for reverse cochlear traveling waves. J. Acoust. Soc. Am. 123, 222–240.
Dong, W., Olson, E.S., 2013. Detection of cochlear amplification and its activation. Biophys. J. 105, 1067–1078.
Dong, W., Olson, E.S., 2016. Two-tone suppression of simultaneous electrical and mechanical responses in the cochlea. Biophys. J. 111, 1805–1815.
Dreiling, F.J., Henson, M.M., Henson Jr, O.W., 2002. The presence and arrangement of type II collagen in the basilar membrane. Hear. Res. 166, 166–180.
Engstrom, H., Wersall, J., 1958. The ultrastructural organization of the organ of Corti and of the vestibular sensory epithelia. Exp. Cell Res. 14, 460–492.
Fallah, E., Strimbu, C.E., Olson, E.S., 2019. Nonlinearity and amplification in cochlear responses to single and multi-tone stimuli. Hear. Res. 377, 271–281.
Fettiplace, R., Kim, K.X., 2014. The physiology of mechanoelectrical transduction channels in hearing. Physiol. Rev. 94, 951–986.
Frank, G., Hemmert, W., Gummer, A.W., 1999. Limiting dynamics of high-frequency electromechanical transduction of outer hair cells. PNAS 96, 4420–4425.
Frost, B.L., Strimbu, C.E., Olson, E.S., 2022. Using volumetric optical coherence tomography to achieve spatially resolved organ of Corti vibration measurements. J. Acoust. Soc. Am. 151, 1115–1124.
Frost, B.L., Strimbu, C.E., Olson, E.S., 2023a. Reconstruction of transverse-longitudinal vibrations in the organ of Corti complex *via* optical coherence tomography. J. Acoust. Soc. Am. 153, 1347–1360.
Frost, B.L., Strimbu, C.E., Olson, E.S., 2023b. Erratum: reconstruction of transverse-longitudinal vibrations in the organ of Corti complex *via* optical coherence tomography [J Acoust Soc Am 153 1347-1360] J. Acoust. Soc. Am. 153, 2537.
Guinan Jr., J.J., 2022. Cochlear amplification in the short-wave region by outer hair cells changing organ-of-Corti area to amplify the fluid traveling wave. Hear. Res. 426, 108641.
He, W., Kemp, D., Ren, T., 2018. Timing of the reticular lamina and basilar membrane vibration in living gerbil cochleae. eLife 7, e37625.
He, W., Burwood, G., Porsov, E.V., Fridberger, A., Nuttall, A.L., Ren, T., 2022a. The reticular lamina and basilar membrane vibrations in the transverse direction in the basal turn of the living gerbil cochlea. Sci. Rep. 12, 19810.
He, W., Burwood, G., Fridberger, A., Nuttall, A.L., Ren, T., 2022b. An outer hair cell-powered global hydromechanical mechanism for cochlear amplification. Hear. Res. 432, 108407.
Iwasa, K.H., Adachi, M., 1997. Force generation in the outer hair cell of the cochlea. Biophys. J. 73, 546–555.
Kale, S., Heinz, M.G., 2010. Envelope coding in auditory nerve fibers following noise-induced hearing loss. JARO 11, 657–673.
Kale, S., Olson, E.S., 2015. Intracochlear scala media pressure measurement: implications for models of cochlear mechanics. Biophys. J. 109, 2678–2688.
Lee, H.Y., Raphael, P.D., Xia, A., Kim, J., Grillet, N., Applegate, B.E., Bowden, A.K.E., Oghalai, J.S., 2016. Two-dimensional cochlear micromechanics measured *in vivo* demonstrate radial tuning with the mouse organ of Corti. J. Neurol. 36, 8160–8173.
Lim, D.J., 1972. Fine morphology of the tectorial membrane: its relationship to the organ of Corti. Arch. Otolaryngol. 96, 199–215.
Lin, N.C., Hendon, C.P., Olson, E.S., 2017. Signal competition in optical coherence tomography and its relevance for cochlear vibrometry. J. Acoust. Soc. Am. 141, 395–405.
Meenderink, S.W.F., Lin, X., Park, B.H., Dong, W., 2022. Sound induced vibrations deform the organ of Corti complex in the low-frequency apical region of the gerbil cochlea for normal hearing. JARO 23, 579–591.
Nankali, A., Wang, Y., Strimbu, C.E., Olson, E.S., Grosh, K., 2020. A role for tectorial membrane mechanics in activating the cochlear amplifier. Sci. Rep. 10, 17620.
Nam, H., Guinan Jr, J.J., 2018. Non-tip auditory-nerve responses that are suppressed by low-frequency bias tones originate from reticular lamina motion. Hear. Res. 358, 1–9.
Narayan, S.S., Temchin, A.N., Recio, A., Ruggero, M.A., 1998. Frequency tuning of basilar membrane and auditory nerve fibers in the same cochleae. Science 282, 1882–1884.
Olson, E.S., 2001. Intracochlear pressure measurements related to cochlear frequency tuning. J. Acoust. Soc. Am. 110, 349–367.
Olson, E.S., Mountain, D.C., 1994. Mapping the cochlear partition's stiffness to its cellular architecture. J. Acoust. Soc. Am. 95, 395–400.
Parsa, A., Webster, P., Kalinec, F., 2012. Deiters cells tread a narrow path: the Deiters cells-basilar membrane junction. Hear Res. 290, 13–20.
Rhode, W.S., 2007. Basilar membrane mechanics in the 6–9kHz region of sensitive chinchilla cochleae. J. Acoust. Soc. Am. 121, 2792–2804.
Sisto, R., Belardinelli, D., Moleti, A., 2021. Fluid focusing and viscosity allow high gain and stability of the cochlear response. J. Acoust. Soc. Am. 150, 4283–4296.
Strimbu, C.E., Wang, Y., Olson, E.S., 2020. Manipulation of the endocochlear potential reveals two distinct types of cochlear nonlinearity. Biophys. J. 119, 2087–2101.
Strimbu, C.E., Olson, E.S., 2022. Salicylate-induced changes in organ of Corti vibrations. Hear Res. 423, 108389.
van der Heijden, M., Joris, P.X., 2003. Cochlear phase and amplitude retrieved from the auditory nerve at arbitrary frequencies. J. Neurosci. 23, 9194–9198.
Versnel, H., Prijs, V.F., Schoonhoven, R., 1997. Auditory-nerve fiber responses to clicks in guinea pigs with a damaged cochlea. J. Acoust. Soc. Am. 101, 993–1009.
Versteegh, C.PC., van der Heijden, M., 2012. Basilar membrane responses to tones and tone complexes: nonlinear effects of stimulus intensity. JARO 13, 785–798.
Wang, Y., Steele, C.R., Puria, S., 2016. Cochlear outer-hair-cell power generation and viscous fluid loss. Sci. Rep. 6, 19475.
Yoon, Y.J., Steele, C.R., Puria, S., 2011. Feed-forward and feed-backward amplification model from cochlear cytoarchitecture: an interspecies comparison. Biophys. J. 100, 1–10.
Zetes, D.E., Tolomeo, J.A ., Holley, M.C., 2012. Structure and mechanics of supporting cells in the guinea pig organ of Corti. PLOS One 7, e4933.
Zhou, W., Jabeen, T., Sabha, S., Becker, J., Nam, J.-H., 2022. Deiters cells act as mechanical equalizers for outer hair cells. J. Neurosci. 42, 8361–8372.